JOURNAL OF THEORETICAL
AND APPLIED MECHANICS
https://doi.org/10.15632/jtam-pl/225473
ONLINE FIRST

# PASSIVE SUSPENSION SYSTEM OF A CHILD SAFETY SEAT – OPTIMIZATION AND ANALYSIS OF VIBRATION ISOLATION EFFECTIVENESS

Natalia Justyna FLOREK*, Igor MACIEJEWSKI, Tomasz KRZYŻYŃSKI

*Faculty of Mechanical and Energy Engineering, Koszalin University of Technology, Koszalin, Poland*
*corresponding author, *natalia.florek@s.tu.koszalin.pl*

The aim of the study is to analyze the vibration damping properties of a passive suspension system for a child car seat that is designed to reduce the impact of vertical accelerations on the child's body during vehicle travel. The motivation for undertaking this research is the absence of vibration isolation solutions dedicated to this group of users, despite the well-documented sensitivity of children to vibrations in the frequency range of 4 Hz to 10 Hz. A physical and mathematical model of the suspension system was developed in the MATLAB/Simulink environment, incorporating springs, hydraulic dampers, bump stops, and nonlinear friction forces. To evaluate vibration isolation performance, acceleration signals were analyzed using the power spectral density (PSD), the root mean square (RMS) value, and the Seat Effective Amplitude Transmissibility (SEAT) factor. In the study, the influence of key structural parameters such as spring stiffness, damping characteristics, and end-stop elements on the effectiveness of vibration reduction was analyzed. Subsequently, a multi-objective optimization procedure was applied to determine the optimal parameters of the suspension system, aiming to minimize the accelerations transmitted to the child seat while maintaining the required design constraints. Simulation results demonstrated that the proposed passive system significantly reduces vibration amplitudes within the low-frequency range and improves the value of the SEAT factor. The results confirm the potential of passive vibration isolation systems for child safety seats and provide a basis for further experimental validation.

**Keywords:** vibration isolation; child car seat; passive suspension system; SEAT factor; power spectral density (PSD).



## 1. Introduction

The primary motivation for undertaking this research is the evident gap in the literature concerning the influence of mechanical vibrations on children traveling in automotive child safety seats. Despite numerous studies addressing vibration isolation systems for driver and adult passenger seats, there is a noticeable lack of investigations that consider the biomechanical specificity of children and their increased susceptibility to vertical vibrations. Table 1 presents the natural frequency ranges of various body parts in children, which differ significantly from the characteristic values reported for adults. These data were compiled, among others, on the basis of studies by Gromadowski and Więckowski (2012), who analyzed the effects of mechanical vibrations on the human body using literature data and industry standards, including ISO 2631, which defines

Ministry of Science and Higher Education
Republic of Poland
WEKTORY NAUKI

This publication has been funded by the Polish Ministry of Science and Higher Education under the "Vectors of Science" programme, project number WNK/SN/0508/2025/01, with project funding of PLN 134,200.00 and total project value of PLN 174,200.00.
The content of this article was presented during the 62nd Symposium "Modelowanie w mechanice" (Modelling in Mechanics), Szczyrk, Poland, March 1–4, 2026.

Table 1. Natural frequency ranges of selected human body parts (Gromadowski & Więckowski, 2012).

| Body part | Natural frequency range [Hz] | Effects of vibration exposure | Group |
|---|---|---|---|
| Head | 4–5 | Headaches, dizziness, discomfort | Child |
| Thorax (chest) | 5–7 | Chest pressure, shallow breathing, pain | |
| Abdomen | 4–8 | Muscle tension | |
| Limbs | 6–8 | Numbness | |
| Spine | 4–9 | Pain | |
| Whole body | 4–10 | Fatigue, nausea, general weakness | |
| Vestibular system (balance) | <6 | Balance disturbances, disorientation | |
| Head | 2–3 | Headache, reduced concentration | Adult |
| Thorax (chest) | 5–7 | Respiratory disturbances | |
| Pelvis / spine | 6–8 | Lower back pain, discomfort | |

comfort limits and permissible levels of vibration exposure. The conclusions drawn from these studies clearly indicate that due to their lower body mass, different anatomical structure, and immature musculoskeletal system, children exhibit significantly higher sensitivity to vibrations, particularly in the vertical direction. The range of frequencies considered harmful to children extends from 4 Hz to 10 Hz, implying that they are exposed to a broader and more intense vibration impact than adults (Wicher & Więckowski, 2010).

The child safety seat suspension system designed within the scope of this study constitutes an innovative solution aimed at reducing the transmission of mechanical vibrations to the user during vehicle operation. The primary objective of developing the passive system was to achieve the highest possible vibration isolation effectiveness while maintaining structural simplicity and operational reliability resulting from the absence of active components. The proposed system is intended to attenuate vibrations within the frequency range characteristic of excitations generated by road surface irregularities and vehicle body dynamics, while simultaneously minimizing accelerations acting on the child's body (Florek & Maciejewski, 2025). The effectiveness of vibration isolation is evaluated using vibration comfort indicators, such as the root mean square (RMS) value of accelerations and the Seat Effective Amplitude Transmissibility (SEAT) factor. As part of the literature review, scientific publications addressing the effects of mechanical vibrations on the human body and the effectiveness of various vibration isolation solutions were analyzed. Based on a critical assessment of the available studies, it can be concluded that children exhibit a biomechanical response to vibration that differs significantly from that of adults, which makes the application of general comfort assessment standards, such as ISO 2631, insufficient for the evaluation of vibration exposure in young passengers (Giacomin, 2005). It has been demonstrated that standard child safety seats do not provide effective vibration isolation; in many cases, amplification of vibration amplitudes is observed within the frequency range of 1.5 Hz to 60 Hz, particularly in the absence of dedicated damping elements (Giacomin, 2000; Bai *et al.*, 2017). An important factor influencing vibration transmission between the vehicle and the child's body is the method of seat installation. The ISOFIX system, in contrast to traditional seatbelt-based mounting, enables a significant reduction in transmitted vibration amplitudes and increases the repeatability and stability of the connection (Wicher & Więckowski, 2010; Gromadowski & Więckowski, 2012). The literature also emphasizes that significant sources of vibrational disturbances may include external factors such as road surface irregularities, wheel imbalance, and wear of vehicle suspension components (Frej & Grabski, 2019; Frej, 2018).

In addition to studies focused directly on child safety seats, broader research on dynamic systems and vibration response has also been conducted. In particular, the analysis of mechanical systems subjected to random and transport-induced excitations has gained significant attention in recent years. Numerous studies have addressed the analysis and modeling of dynamic systems subjected to vibration excitation, including transport-related vibrations and random loading conditions. Research conducted by Duda *et al.* (2020), Hryciów *et al.* (2021), and Łagoda (2001) highlights the importance of accurate modeling of dynamic responses and energy transfer mechanisms in systems exposed to stochastic excitations. These approaches provide a valuable background for the analysis and optimization of vibration isolation systems. Finite element modeling has also been widely used in seat-structure and human–seat interaction analyses. Zhang *et al.* (2015) developed an FE model of a car seat with an occupant to predict vertical vibration transmissibility, while Alawneh *et al.* (2022) reviewed FE approaches for human–seat interaction. These studies confirm the importance of numerical modeling in seating comfort analyses, although the present work adopts a lumped-parameter model to enable efficient multi-variant optimization.

The literature review clearly indicates that, despite numerous studies addressing vibration comfort in adult vehicle occupants, passive systems dedicated specifically to child safety seats remain lacking. Existing designs do not account for the biomechanical specificity of young children, which results in increased transmission of vibrations to the user's body. The suspension system developed within the scope of this study addresses this research gap by focusing on a passive solution with optimized damping and stiffness characteristics tailored to the vibration sensitivity of children. Current vibration comfort assessment standards, such as ISO 2631 (International Organization for Standardization, 1997; 2001; 2018), were developed primarily for adult users and do not account for the biomechanical specificity of children or the distinct natural frequencies of individual body segments. Based on an analysis of recent scientific studies, it can be unequivocally stated that children exhibit a markedly different biomechanical response to mechanical vibrations compared to adults. Giacomin (2005) demonstrated that standard child seat vehicle systems transmit vibrations of significantly higher amplitude to the child's body, particularly in low-frequency bands. Furthermore, in studies on the so-called *apparent mass* of children, Giacomin (2004) confirmed that their biodynamic response to vibration differs substantially from that of adults. Bai *et al.* (2017) analyzed the effects of vibration on different segments of the spine and showed that the sensitivity of the lumbar vertebrae in children to specific vibration frequencies is considerably higher than in adults. Consequently, numerous studies question the adequacy of applying general standards such as ISO 2631 to the assessment of vibration comfort in children traveling in vehicles. Nilsson (2005) and Florek and Maciejewski (2025) argue that although these standards are widely used in analyses of adult vibration exposure, they do not account for the physiological and biomechanical differences present in children, which may lead to an incorrect assessment of health-related risks. A similar position is presented by Zuska *et al.* (2021), who suggest the need to revise existing standards or to develop child-specific counterparts.

Another important conclusion, confirmed by multiple studies, concerns the ineffectiveness of standard child safety seats in isolating vibrations. Giacomin (2005) and Frej and Grabski (2023) demonstrated that, rather than attenuating vibrations, many commercially available child seats amplify vibration amplitudes. Wicher and Więckowski (2010) and Gromadowski and Więckowski (2012) further indicate that the absence of damping elements in a child safety seat may lead to resonance effects and increased transmission of vibrations to the child's body. The effectiveness of vibration attenuation is also strongly influenced by the method of seat installation. Improved stability and repeatability of installation were also reported, which translates into reduced exposure of the child to unwanted vibrations. The literature additionally highlights external sources of vibration, such as road surface irregularities, wheel imbalance, and wear of vehicle suspension components. Frej (2018) demonstrated that the technical condition of the vehicle has a direct impact on the level of vibrations transmitted to the cabin interior and indirectly to the child. Against the background of these findings, a clear research gap emerges in the area of dedicated passive vibration protection systems for the youngest vehicle occupants. Addressing this deficiency may be achieved through the development of a passive damping system with properties tailored to the biomechanical characteristics of children, which constitutes the objective of the engineering solution proposed in this study. In response to these limitations, the development of a dedicated suspension system for child safety seats is proposed, with the primary goal of reducing the transmission of vertical vibrations to the child's body (Florek & Maciejewski, 2025). As part of the research, both a physical and a mathematical model of the system were developed in the MATLAB/Simulink environment, incorporating excitation forces generated by road surface irregularities as well as the dynamic response of the suspension system. The model was calibrated for the frequency range characteristic of children aged 0–6 years, enabling an assessment of vibration attenuation effectiveness under simulation conditions.

## 2. Physical and mathematical model of the passive system

### 2.1. Physical model

Figure 1 presents a simplified physical model of the passive suspension system of a child safety seat. The model consists of a single lumped mass $m_1$, representing the combined system of the child safety seat and the child's body:

$$m_1 q_{1z} = -F_{sz} - F_{bz} - F_{dz} - F_{fz}. \tag{2.1}$$

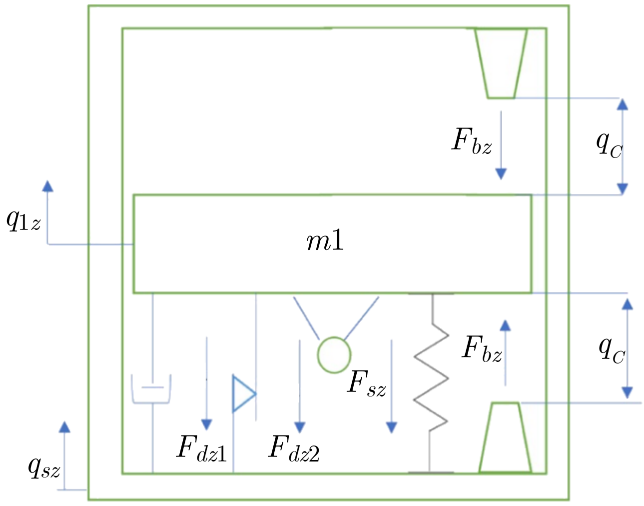


Fig. 1. Physical model of the passive suspension system of a child safety seat (Maciejewski *et al.*, 2020).

The lumped mass $m_1$ is subjected to passive forces acting within the system: $F_{sz}$, the spring force, responsible for storing elastic energy in the system and defining its stiffness; $F_{dz1}$, the damping force generated by fluid flow in the hydraulic damper during the relative motion between the child seat and the base; $F_{bz}$, the force produced by the end stops (elastic bumpers), which limit the maximum displacement of the mass and prevent impacts at extreme positions; and $F_{fz}$, the friction force resulting from the contact and guidance of moving components, providing a stabilizing effect at low relative velocities. The variable $q_{1z}$ denotes the vertical displacement of the mass $m_1$, while $q_{sz}$ refers to the displacement of the suspension base. The difference $q_{1z} - q_{sz}$ defines the relative displacement of the system and constitutes the basis for calculating the elastic and damping forces. In the contact region with the end stops, an additional variable $q_C$ is introduced, representing the activation threshold of the bumper, beyond which the nonlinear force characteristic $F_{bz}$ becomes effective. The model assumes a single degree of freedom, which enables a precise analysis of vertical vibrations of the vibration isolation system in response to base excitation $q_{sz(t)}$.

### 2.2. Mathematical model

The mathematical description of the passive system comprises four main force components responsible for its dynamic properties: elasticity, damping, displacement limitation, and friction.

#### *2.2.1. Spring force*

The relationship between the relative displacement of the system $(q_{1z} - q_{sz})$ and the elastic force is expressed by the following relation:

$$F_{sz} = \frac{G_s\, d_s^4}{8\, n_s\, D_s^3}(q_{1z} - q_{sz}), \tag{2.2}$$

where $G_s$ denotes the shear modulus of the spring material, $d_s$ is the spring wire diameter, $D_s$ is the mean coil diameter, and $n_s$ represents the number of active coils. This relationship describes the classical linear model of a helical spring, in which the force is proportional to the spring deflection. The geometric parameters of the wire and the coil have a crucial influence on the effective stiffness of the system, which in the subsequent part of this study constituted the basis for the structural optimization process (Krzyzynski *et al.*, 2019).

#### *2.2.2. End-stop bumper force*

The end-stop bumper force was formulated as a piecewise function of the relative displacement between the suspended mass and the system base, enabling the representation of successive operating phases: no contact, a linear response, and a nonlinear behavior at large deflections:

$$\begin{aligned} &F_{bz} = 0 && \text{for} \quad |r| \le q_C + \delta, \\ &F_{bz} = \operatorname{sgn}(r)\, c_{b1}(|r| - q_C - \delta) && \text{for} \quad q_C + \delta < |r| \le q_T, \\ &F_{bz} = \operatorname{sgn}(r)\, c_{b3}(|r| - q_T - \delta)^3 + c_{b1}(|r| - q_C - \delta)] && \text{for} \quad |r| > q_T + \delta, \end{aligned} \tag{2.3}$$

$$F_{nr} = c_{b3}(q_{1z} - q_{sz} - q_T - \delta) + c_{b1}(q_{1z} - q_{sz} - q_C - \delta), \tag{2.4}$$

$$F_{lr} = c_{b1}(q_{1z} - q_{sz} - q_C - \delta), \tag{2.5}$$

where $r = q_{1z} - q_{sz}$.

The force generated by the end-stop bumper, which serves as a suspension travel limiter, is described by Eq. (2.3). Its magnitude depends on the relative displacement between the suspended mass and the system base, denoted as $(q_{1z} - q_{sz})$. In the model, it is assumed that for small displacement values satisfying the condition $\mid q_{1z} - q_{sz} \mid \le q_C + \delta$, the bumper does not generate any reaction force, which corresponds to the absence of contact between the bumper and the moving platform. Once the threshold value $(q_C + \delta)$ is exceeded, the bumper enters a linear operating region. In this range, the force increases proportionally with displacement and is described by $F_{bz} = c_{b1}(q_{1z} - q_{sz} - q_C - \delta)$. The linear elastic model applied in this region represents the behavior of a pre-compressed elastomer or rubber stop, which begins to transmit mechanical loads only after the assembly clearance has been eliminated. With further increase in deflection, when the condition $\mid q_{1z} - q_{sz} \mid > q_T + \delta$ is satisfied, the element enters a nonlinear operating region. The bumper characteristic then assumes a cubic form and is expressed as $F_{bz} = c_{b3}(q_{1z} - q_{sz} - q_T - \delta)^3 + c_{b1}(q_{1z} - q_{sz} - q_C - \delta)$. The inclusion of the nonlinear term enables an accurate representation of the rapid stiffness increase characteristic of rubber and polyurethane bumpers in the final stage of deformation. Additionally, for situations involving dynamic impact against the travel limiter, an impact reaction force $F_{nr}$ was introduced and is described by Eq. (2.4). This term accounts for the elastic rebound effect occurring during rapid contact with the travel limit and enables the representation of an asymmetric force characteristic during the separation phase of the bumper from the mating surface (Krzyzynski *et al.*, 2019).

### *2.2.3. Damper force*

The damping force generated by the hydraulic damper is described using a model based on flow losses of the working fluid through a throttling orifice. The value of the damping force $F_{dz}$ depends on the direction of flow (chamber $B \to A$ or $A \to B$) as well as on the relative velocity of the piston with respect to the base, which corresponds to the forced oil flow velocity inside the damper. It is assumed that for a positive relative velocity $\dot{q}_{1z} - \dot{q}_{sz} > 0$, the fluid flows from chamber $B$ to chamber $A$, whereas for $\dot{q}_{1z} - \dot{q}_{sz} < 0$, the flow occurs from chamber $A$ to chamber $B$. The damper force is expressed by the following relationship:

$$\begin{aligned} F_{dz} &= \zeta_{B\to A} \cdot \rho_0/2 \cdot (A_B v/A_0)^2 \cdot A_B \qquad \text{for} \quad v > 0, \\ F_{dz} &= -\zeta_{A\to B} \cdot \rho_0/2 \cdot (A_A v/A_0)^2 \cdot A_A \quad \text{for} \quad v < 0, \end{aligned} \tag{2.6}$$

where $v = \dot{q}_{1z} - \dot{q}_{sz}$ and the minus sign in the second case ensures that the damping force acts in the direction opposite to the motion, i.e., the force always acts as a resistance to the flow of kinetic energy in the system:

$$\begin{aligned} -\zeta_{(B\to A)} &= 64/\mathrm{Re}_{(B\to A)} \cdot (\alpha_o + l_o/d_o) && \text{for} \quad 64/\mathrm{Re}_{(B\to A)} \cdot (\alpha_o + l_o/d_o) > 1.8, \\ -\zeta_{(B\to A)} &= 1.8 && \text{for} \quad 64/\mathrm{Re}_{(B\to A)} \cdot (\alpha_o + l_o/d_o) \le 1.8, \\ -\zeta_{(A\to B)} &= 64/\mathrm{Re}_{(A\to B)} \cdot (\alpha_o + l_o/d_o) && \text{for} \quad 64/\mathrm{Re}_{(A\to B)} \cdot (\alpha_o + l_o/d_o) > 1.8, \\ -\zeta_{(A\to B)} &= 1.8 && \text{for} \quad 64/\mathrm{Re}_{(A\to B)} \cdot (\alpha_o + l_o/d_o) \le 1.8. \end{aligned} \tag{2.7}$$

The coefficients $\zeta_{(B\to A)}$ and $\zeta_{(A\to B)}$ describe flow losses depending on the flow regime (laminar or turbulent) and are expressed as functions of the Reynolds number. In the model, a Reynolds-number-dependent formulation was adopted with a lower bound of $\zeta = 1.8$, which ensures numerical stability and represents the minimum level of flow losses. The Reynolds numbers for both flow directions were determined using the following relations:

$$\mathrm{Re}_{(B->A)} = \frac{4[A_B(\dot{q}_{1z} - \dot{q}_{sz})]}{d_o \pi v_o}, \qquad \mathrm{Re}_{(A->B)} = \frac{4[A_A(\dot{q}_{1z} - \dot{q}_{sz})]}{d_o \pi v_o}. \tag{2.8}$$

The adopted formulation enables the inclusion of the nonlinear dependence of the damping force on the relative velocity (quadratic velocity term in the dynamic component) as well as the influence of flow regime transitions through the function $\zeta(\mathrm{Re})$. Consequently, the model reproduces the typical behavior of hydraulic dampers, characterized by relatively low damping forces at small velocities and a rapidly increasing flow resistance at higher velocities, which is particularly important for the attenuation of vibrations with higher dynamic intensity (Krzyzynski *et al.*, 2019).

### *2.2.4. Friction force*

Friction phenomena in the system were described using an extended Stribeck model with a Coulomb friction term, which enables a smooth transition from static to dynamic friction and eliminates discontinuities at velocities close to zero:

$$F_{fz} = \sqrt{2\mathrm{e}(F_{brk} - F_c)} \cdot \exp\left(-\left(\frac{q_{1z} - q_{sz}}{V_{\mathrm{st}}}\right)2\right) \cdot \frac{q_{1z} - q_{sz}}{V_{\mathrm{st}}} + F_c \cdot \tanh\left(\frac{q_{1z} - q_{sz}}{V_{\mathrm{coul}}}\right), \tag{2.9}$$

where $F_{brk}$ denotes the maximum static friction force, $F_c$ represents the dynamic (Coulomb) friction force, and $V_{\mathrm{st}}$ and $V_{\mathrm{coul}}$ are characteristic velocities describing the transition between static and dynamic friction states. The application of this model enables an accurate representation of micro-scale friction phenomena occurring in the guides and articulated joints of the child safety seat, which has a significant influence on the attenuation of low-amplitude vibrations (Krzyzynski *et al.*, 2019).

## 3. Influence of selected model parameters on changes in the viscoelastic characteristics of the suspension system

As a part of the conducted analyses, the influence of key structural parameters of passive components on the viscoelastic characteristics of the passive suspension system of a child safety seat was investigated. For this purpose, four decision variables were defined as follows: the spring wire diameter $d_s = 0.5\,\text{mm}$ to $3\,\text{mm}$, the bumper activation parameter $\delta = -15\,\text{mm}$ to $5\,\text{mm}$, the damper orifice diameter $d_o = 0.5\,\text{mm}$ to $5\,\text{mm}$, and the dynamic friction force $F_c = 12\,\text{N}$ to $50\,\text{N}$. For each of these parameters, force–displacement or force–velocity characteristics were generated (Fig. 2 to Fig. 5), which enabled an assessment of their influence on the dynamic properties of the system and the identification of parameters with the greatest significance for vibration isolation effectiveness.

The analysis of the first parameter (Fig. 2), namely the spring wire diameter $d_s = 0.5\,\text{mm}$ to $3\,\text{mm}$, has shown that variations in this dimension have a pronounced effect on the stiffness characteristic. In accordance with helical spring theory, the stiffness increases proportionally to the fourth power of the wire diameter, which is clearly reflected in the obtained results. With increasing $d_s$, a monotonic increase in the slope of the force–displacement characteristic is observed, corresponding to a substantial increase in spring stiffness. This leads to a reduction in the relative displacement of the suspended mass. However, it simultaneously results in increased transmission of low-frequency vibrations. Lower values of the spring wire diameter $d_s$ improve vibration comfort by increasing the system's ability to reduce acceleration levels. However, this improvement is achieved at the expense of a higher risk of reaching the allowable limits of relative displacement. Therefore, the range $d_s = 0.5\,\text{mm}$ to $3\,\text{mm}$ was selected as a decision variable in the optimization process, enabling precise tuning of the system stiffness.

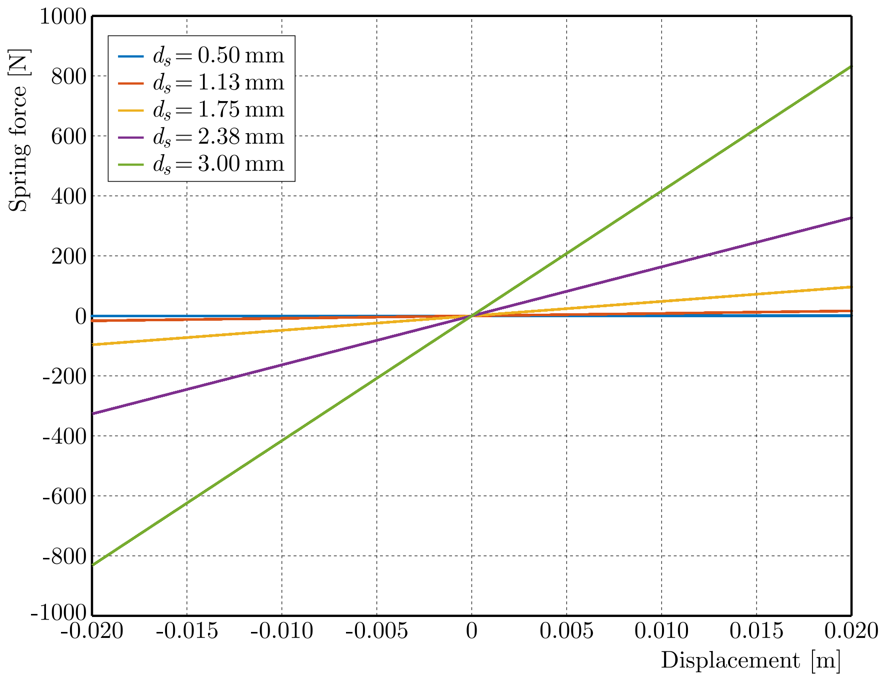


Fig. 2. Spring characteristic for different $d_s$.

The next analyzed component was the end-stop bumper (Fig. 3), for which the influence of the activation parameter $\delta = -15\,\text{mm}$ to $5\,\text{mm}$, governing the onset of contact between the suspended mass and the travel limiter, was evaluated. The bumper characteristic consists of a no-contact region, a linear force growth region, and a dynamically increasing nonlinear region. The analysis has confirmed that more negative values of $\delta$ delay the onset of force generation by

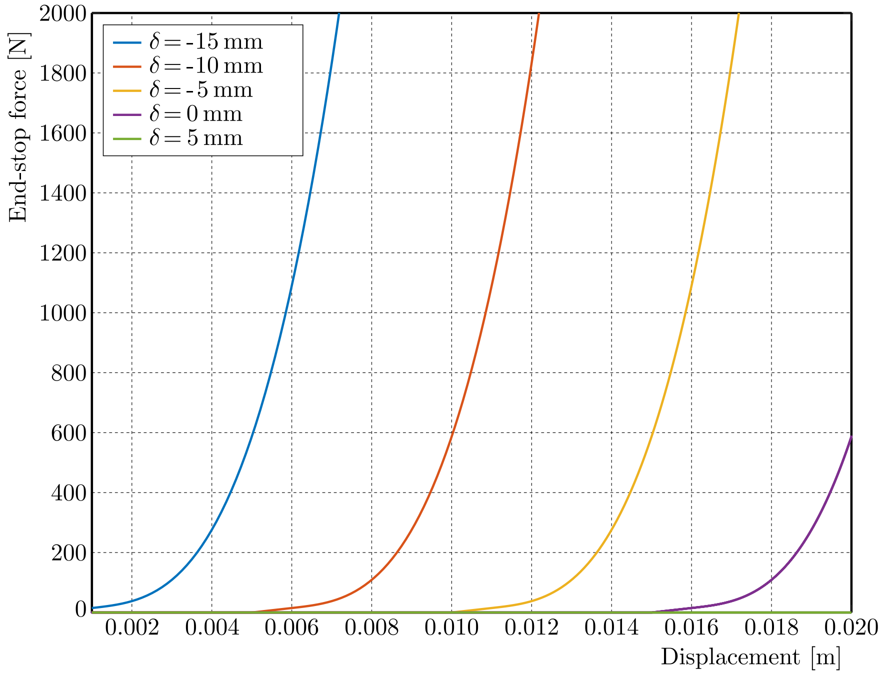


Fig. 3. End-stop bumper characteristic for different $\delta$.

the bumper, thereby increasing the effective linear operating range of the entire suspension system. As a result, the system becomes more compliant for small displacements, which improves its vibration isolation properties in the low-frequency range. Once the activation threshold determined by $\delta = -15\,\text{mm}$ to $5\,\text{mm}$ is exceeded, a rapid increase in stiffness is observed, providing protection against excessive deflection and contact with structural constraints. This behavior is consistent with that of real elastomeric bumpers, in which an intentional initial assembly clearance is commonly applied.

The influence of the damper orifice diameter $d_o = 0.5\,\text{mm}$ to $5\,\text{mm}$ (Fig. 4) was analyzed with respect to the hydraulic damper characteristics. The obtained force–velocity curves clearly

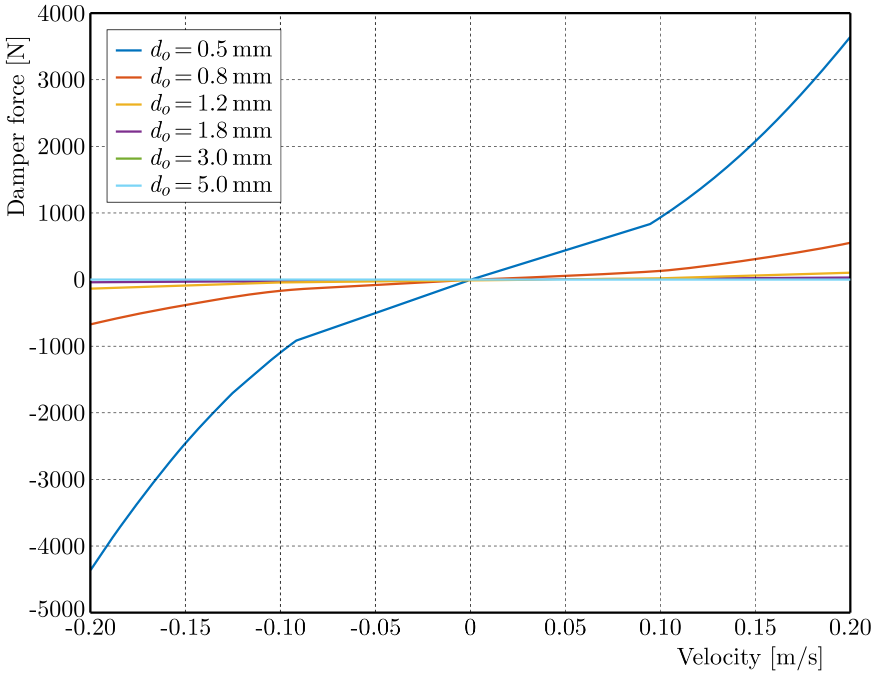


Fig. 4. Damper characteristic for different $d_o$.

indicate a strong nonlinear dependence of the damping force on the relative piston velocity. A reduction in $d_o$ leads to a significant increase in fluid flow resistance and, consequently, to higher damping forces, particularly in the velocity range corresponding to the transition from laminar to turbulent flow. This behavior confirms the correct representation of the damper in the mathematical model, as real hydraulic dampers exhibit a similar increase in force as a function of velocity. Higher damping forces improve the attenuation of vibrations in the medium- and high-frequency ranges. However, an excessive flow resistance resulting from small orifice diameters within the range $d_o = 0.5$ mm to 5 mm leads to an increase in the dynamic stiffness of the system, which may deteriorate comfort under large-amplitude excitations.

The final analyzed parameter was the dynamic friction force (Fig. 5), $F_c = 12$ N to 50 N, describing friction characteristics in the system guides and modeled using the extended Stribeck formulation. The force–velocity relationship showed that increasing $F_c$ enhances low-velocity damping, which plays an important role in stabilizing motion under small excitations. Higher values of $F_c$, including the range $F_c = 12$ N to 50 N considered in the analysis, reduce the amplitude of free oscillations and limit vibrations occurring near the static equilibrium position. At the same time, excessive friction promotes the occurrence of stick-slip phenomena, leading to abrupt displacement changes and increased vibration transmission within certain frequency bands. For this reason, the selection of $F_c$ constituted a key stage of the subsequent optimization process, enabling a compromise between motion stabilization and smooth system operation.

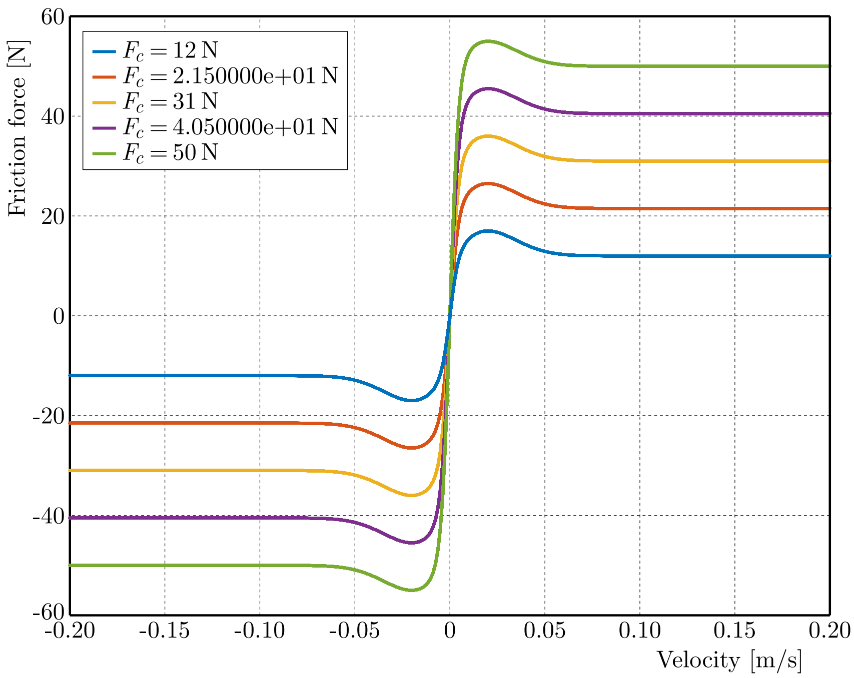


Fig. 5. Friction force characteristic as a function of velocity for different $F_c$.

The analysis of the four model parameters has clearly demonstrated that each of them has a significant influence on the resulting dynamic properties of the passive system. The spring wire diameter $d_s$ determines the fundamental stiffness of the system, the parameter $\delta$ controls the transition to the nonlinear operating regime of the end stop, the orifice diameter $d_o$ governs the viscous damping characteristics, while the friction force $F_c$ is responsible for low-velocity damping and motion stability. Understanding the interaction of these parameters provides the basis for the appropriate selection of passive component properties and enables an effective optimization of the system with respect to minimizing the SEAT factor and limiting the relative displacement RS (relative stroke).

## 4. Excitation signals and evaluation criteria

To evaluate the effectiveness of the proposed passive system, it was necessary to apply excitation signals representative of the real operating conditions of a child safety seat in a vehicle. In the numerical analyses, a time-domain signal with characteristics close to white noise in the frequency range from 0.5 Hz to 10 Hz was used, corresponding to the typical frequency band encountered during vehicle operation on uneven road surfaces. The spectrum of the signal, obtained from the power spectral density (PSD), confirms the broadband nature of the excitation and a relatively uniform loading of the system over the entire analyzed frequency range. The applied excitation signal corresponds to conditions commonly used in laboratory testing of child safety seats as well as in field experiments, while simultaneously enabling the identification of changes in the dynamic characteristics of the system resulting from variations in structural parameters (Fig. 6). Such a signal provides a good approximation of real random vertical vibrations and is widely used in the analysis of vibration isolation systems due to the absence of dominant frequencies that could bias the assessment of vibration transmissibility.

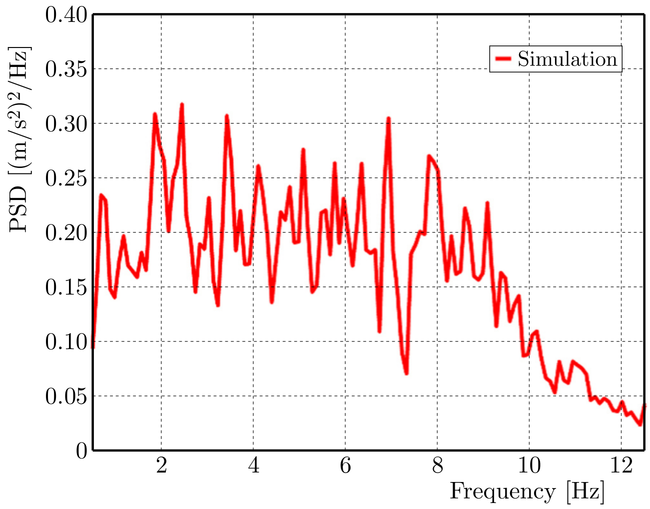


Fig. 6. Power spectral density of the excitation signal inducing vibratory motion.

The damping performance of the proposed system was evaluated using two indicators: the SEAT coefficient and the maximum relative displacement RS:

$$\mathrm{SEAT} = \frac{(q_{1z})_{\mathrm{RMS}}}{(q_{sz})_{\mathrm{RMS}}}. \tag{4.1}$$

The SEAT factor is a measure of the effective transmission of vibrations through the system and is defined as the ratio of the RMS value of the weighted acceleration on the isolated side to the corresponding value on the excitation side. The frequency weighting was selected in accordance with the recommendations of ISO 2631, enabling the consideration of the varying sensitivity of the human body to vibrations across different frequency bands. The SEAT index enables a direct assessment of vibration reduction in terms closely related to user comfort and is a standard analytical tool in studies of vibration isolation systems. Values of SEAT $< 1$ indicate an isolating effect of the system, whereas SEAT $> 1$ signify vibration amplification within specific frequency ranges. The second indicator used to evaluate system performance was the relative displacement RS, defined as the maximum positional difference between the isolated mass (the child safety seat and the child) and the excitation base:

$$\mathrm{RS} = \max_{t\in[0,tk]}\big(q_{1z(t)} - q_{sz(t)}\big) - \min_{t\in[0,tk]}\big(q_{1z(t)} - q_{sz(t)}\big). \tag{4.2}$$

The relative displacement RS was used as a structural safety indicator, defining the suspension travel required to avoid excessive loading of the end stops or contact with structural limits. The combined use of SEAT and RS enables the simultaneous evaluation of vibration comfort and safe operating range, which is essential in the optimization of passive vibration isolation systems.

## 5. Optimization of vibration isolation performance of the passive system and optimal characteristics of passive components

The optimization of the vibration isolation performance of the passive system was carried out using a deterministic full factorial parametric search. Four decision variables were considered: the spring wire diameter $d_s$, the bumper activation parameter $\delta$, the hydraulic damper orifice diameter $d_o$, and the dynamic friction force $F_c$. Each variable was discretized into 15 equally spaced values within the adopted design range: $d_s = 0.5\,\text{mm}$ to $3\,\text{mm}$, $\delta = -15\,\text{mm}$ to $5\,\text{mm}$, $d_o = 0.5\,\text{mm}$ to $5\,\text{mm}$, and $F_c = 12\,\text{N}$ to $50\,\text{N}$. Consequently, 50 625 combinations of passive component parameters were analyzed.

For each parameter combination, a numerical simulation of the passive suspension system was performed in MATLAB/Simulink. The SEAT coefficient and the RS were calculated and stored as the evaluation criteria. The optimization problem was formulated as the simultaneous minimization of the SEAT coefficient, representing vibration transmission to the child's body, and the RS, representing the suspension travel required for safe operation. Since a deterministic full factorial search was used, no stochastic convergence criterion was required; the procedure was completed after all predefined parameter combinations had been evaluated. The Pareto-optimal solutions were selected from the complete set of admissible results. First, the solutions corresponding to the minimum SEAT value and the minimum RS value were identified. Then, ten constraint levels of RS were defined between these limiting cases. For each RS constraint, the solution with the lowest SEAT value was selected. This procedure resulted in a set of ten Pareto-optimal solutions representing different compromises between vibration isolation effectiveness and suspension travel limitation. The resulting Pareto-optimal solutions in the SEAT–RS evaluation criteria space are presented in Fig. 9. The spring characteristics obtained as a result of the optimization process (Fig. 7) indicate the necessity of achieving a compromise between

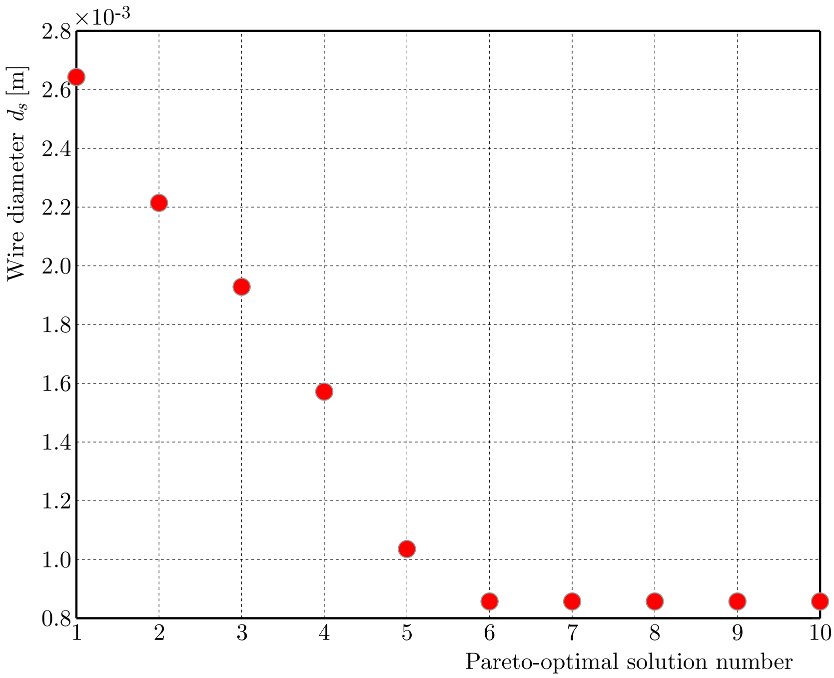


Fig. 7. Optimal characteristics of passive components – spring.

sufficiently low stiffness, which promotes the reduction of low-frequency vibrations, and adequate global system stiffness, which limits excessive relative displacements. In the case of the hydraulic damper (Fig. 11), the optimal parameter values lead to a nonlinear increase in the damping force with increasing relative motion velocity. This behavior is particularly advantageous, as it enables effective dissipation of vibration energy in the medium- and high-frequency ranges without causing excessive system stiffening during slow position changes. The optimized end-stop bumper characteristic (Fig. 10) allows for a delayed activation of the nonlinear portion of the limiter response, ensuring high compliance of the system in the range of small deflections. Only at larger displacements does the reaction force increase rapidly, effectively protecting the

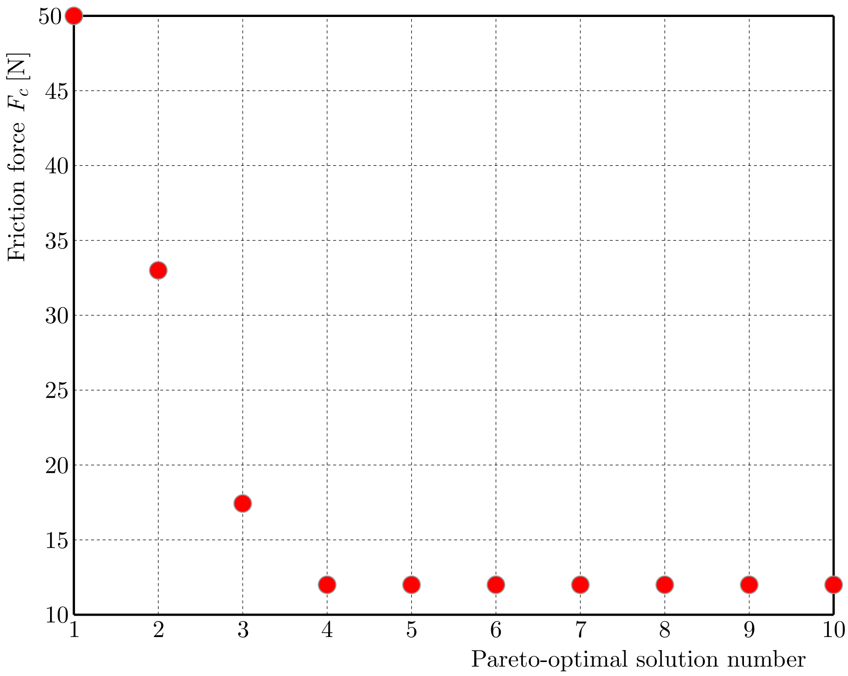


Fig. 8. Optimal characteristics of passive components – friction.

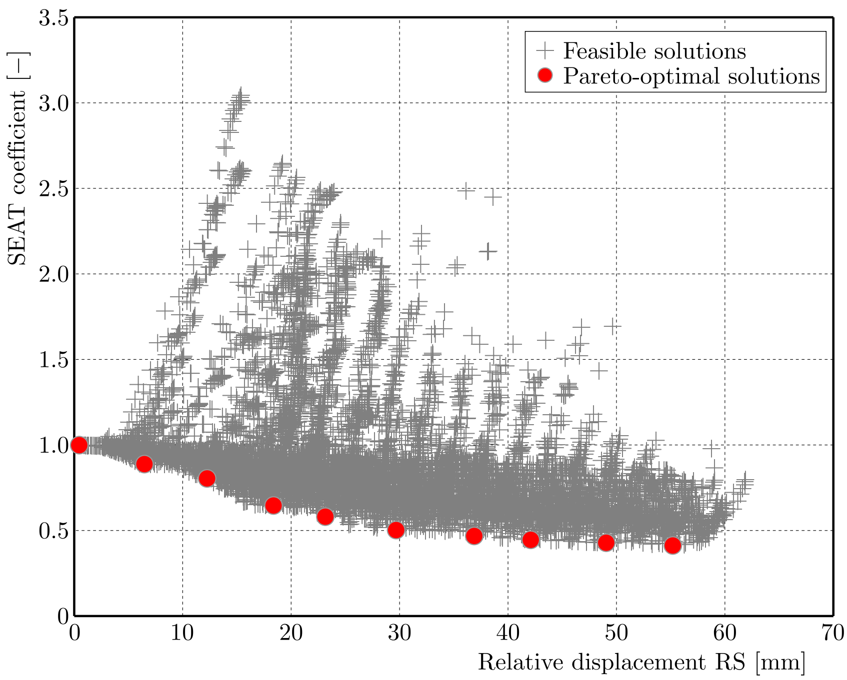


Fig. 9. Optimal characteristics of passive components – evaluation criteria space.

system against exceeding the allowable suspension travel. In turn, the appropriately selected value of the dynamic friction force (Fig. 8) provides motion stabilization at low velocities while simultaneously limiting the risk of stick-slip phenomena and the associated abrupt displacement changes. Such a friction damping characteristic supports effective attenuation in the low-velocity range and enhances the overall stability of the system. The frequency-domain results (Fig. 12) indicate a reduction in vibration transmissibility in the range of approximately 1 Hz to 10 Hz, which is particularly relevant for child comfort. For the selected optimal passive configuration, the SEAT coefficient was reduced to 0.47, while the RS remained equal to 36.8 mm. These values

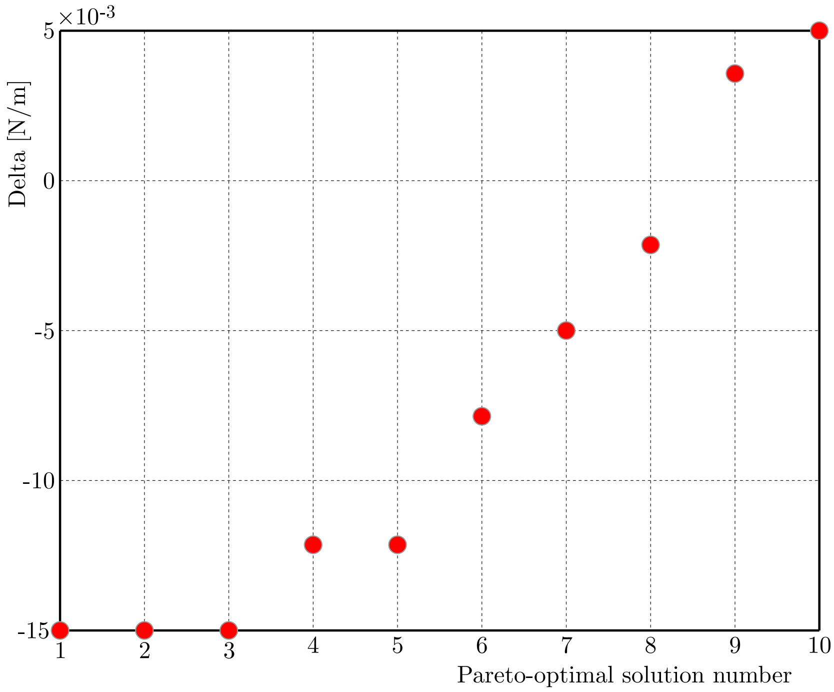


Fig. 10. Optimal characteristics of passive components – end-stop bumpers.

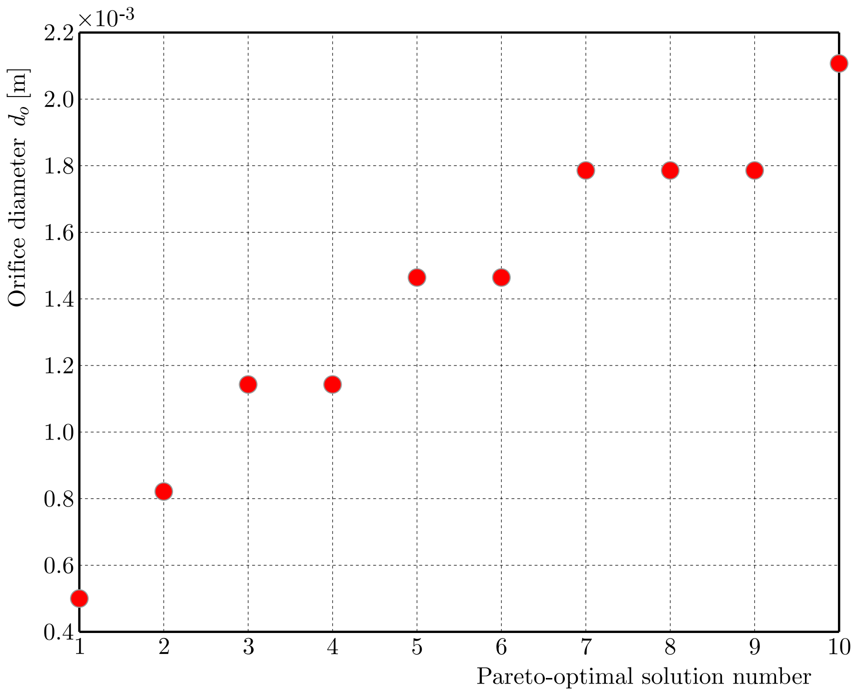


Fig. 11. Optimal characteristics of passive components – damper.

confirm that the optimized passive suspension system provides effective vibration attenuation while maintaining the required suspension travel within the admissible operating range. The resulting parameter set may serve as a reference point for further experimental validation and comparison with semi-active and active systems.

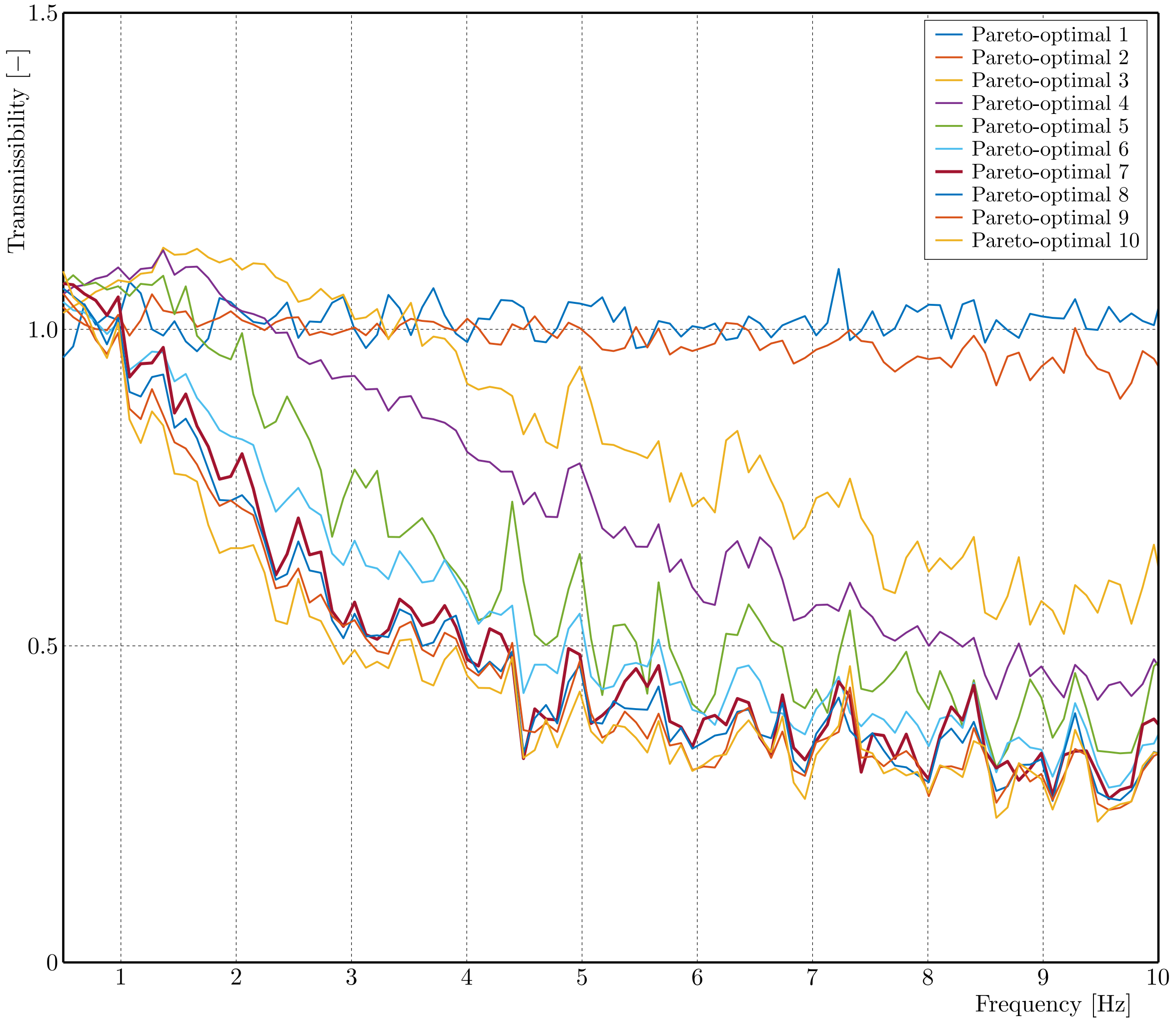


Fig. 12. Vibration transmissibility functions of selected Pareto-optimal solutions.

## 6. Conclusions

The conducted studies have confirmed that the dynamic response of the passive suspension system of a child safety seat depends mainly on the parameters related to elasticity, damping, and friction. The numerical model reproduced the behavior of elastic, damping, friction, and end-stop components, and the obtained force–displacement and force–velocity characteristics were consistent with the physical properties of these elements. The optimization of passive parameters resulted in a measurable improvement in vibration isolation performance. For the selected optimal passive configuration, the SEAT coefficient reached 0.47, while the RS was 36.8 mm. This confirms that the optimized passive system can reduce vibration transmission while maintaining the displacement of the suspended mass within a safe operating range. The present study was limited to numerical modeling, sensitivity analysis, and optimization. Future work will include field tests using an anthropomorphic dummy equipped with acceleration sensors to compare the numerical predictions with experimental measurements and to support the development of semi-active and active vibration isolation systems for child safety seats.

## References


1. Alawneh, O., Zhong, X., Faieghi, R., & Xi, F. (2022). Finite element methods for modeling the pressure distribution in human body–seat interactions: A systematic review. *Applied Sciences*, *12*(12), Article 6160. https://doi.org/10.3390/app12126160

2. Bai, X.-X., Xu, S.-X., Cheng, W., & Qian, L.-J. (2017). On 4-degree-of-freedom biodynamic models of seated occupants: Lumped-parameter modeling. *Journal of Sound and Vibration*, *402*, 122–141. https://doi.org/10.1016/j.jsv.2017.05.018

3. Duda, S., Dudek, O., Gembalczyk, G., & Machoczek, T. (2020). Developing a test site for testing the suspension of vehicles with omnidirectional wheels. *Vibrations in Physical Systems*, *31*(3), 2020304-1–2020304-8. https://doi.org/10.21008/j.0860-6897.2020.3.04

4. Florek, N.J., & Maciejewski, I. (2025). The impact of vibrations on the comfort and safety of children in car seats: A review of current knowledge. *Vibrations in Physical Systems*, *36*(2), 2025211-1–2025211-8. https://doi.org/10.21008/j.0860-6897.2025.2.11

5. Frej, D. (2018). Influence of wheel imbalance on driver's vibration comfort – front and rear axle (in Polish). In M. Bogusz, M. Wojcieszak, & P. Rachwał (Eds.), *Poszerzamy Horyzonty* (Vol. IX, pp. 531–553). https://www.konferencjenaukowe.com.pl/monografia9.pdf

6. Frej, D., & Grabski, P. (2019). The impact of the unbalanced rear wheel on the vibrating comfort of the child seat. *Transportation Research Procedia*, *40*, 678–685. https://doi.org/10.1016/j.trpro.2019.07.096

7. Frej, D., & Grabski, P. (2023). Trends in choosing the right child seat – survey research. *Transportation Research Procedia*, *74*, 1308–1317. https://doi.org/10.1016/j.trpro.2023.11.276

8. Giacomin, J. (2000). Some observations regarding the vibrational environment in child safety seats. *Applied Ergonomics*, *31*(2), 207–215. https://doi.org/10.1016/s0003-6870(99)00034-4

9. Giacomin, J. (2004). Apparent mass of small children: experimental measurements. *Ergonomics*, *47*(13), 1454–1474. https://doi.org/10.1080/00140130412331290817

10. Giacomin, J. (2005). Absorbed power of small children. *Clinical Biomechanics*, *20*(4), 372–380. https://doi.org/10.1016/j.clinbiomech.2004.12.001

11. Gromadowski, T., & Więckowski, D. (2012). Analysis of vertical vibration affecting the child in a car with the use of the white noise signal input (in Polish). *Postępy Nauki i Techniki*, *14*, 83–94.

12. Hryciów, Z., Małachowski, J., Rybak, P., & Wiśniewski, A. (2021). Research of vibrations of an armoured personnel carrier hull with FE implementation. *Materials*, *14*(22), Article 6807. https://doi.org/10.3390/ma14226807

13. International Organization for Standardization. (1997). *Mechanical vibration and shock – Evaluation of human exposure to whole-body vibration. Part 1: General requirements* (ISO Standard No. 2631-1:1997). https://www.iso.org/standard/7612.html

14. International Organization for Standardization. (2001). *Mechanical vibration and shock – Evaluation of human exposure to whole-body vibration. Part 4: Guidelines for the evaluation of the effects of vibration and rotational motion on passenger and crew comfort in fixed-guideway transport systems* (ISO Standard No. 2631-4:2001). https://www.iso.org/standard/32178.html

15. International Organization for Standardization. (2018). *Mechanical vibration and shock – Evaluation of human exposure to whole-body vibration. Part 5: Method for evaluation of vibration containing multiple shocks* (ISO Standard No. 2631-5:2018). https://www.iso.org/standard/50905.html

16. Krzyzynski, T., Maciejewski, I., Meyer, L., & Meyer, H. (2019). *Modelling and control design of vibration reduction systems. Methods and procedures of selecting vibro-isolation properties.* Springer. https://doi.org/10.1007/978-3-030-03047-6

17. Łagoda, T. (2001). Energy models for fatigue life estimation under uniaxial random loading. Part I: The model elaboration. *International Journal of Fatigue*, *23*(6), 467–480. https://doi.org/10.1016/S0142-1123(01)00016-0

18. Maciejewski, I., Zlobinski, M., Krzyzynski, T., & Glowinski, S. (2020). Vibration control of an active horizontal seat suspension with a permanent magnet synchronous motor. *Journal of Sound and Vibration*, *488*, Article 115655. https://doi.org/10.1016/j.jsv.2020.115655

19. Nilsson, M. (2005). Health risk aspects and comfort for infants in infant seats for cars. *VTI Notat 24-2005. Swedish National Road and Transport Research Institute (VTI).*

20. Wicher, J., & Więckowski, D. (2010). Influence of vibrations of the child seat on the comfort of child's ride in a car. *Eksploatacja i Niezawodność – Maintenance and Reliability*, *4*, 102–110.

21. Zhang, X., Qiu, Y., & Griffin, M.J. (2015). Developing a simplified finite element model of a car seat with occupant for predicting vibration transmissibility in the vertical direction. *Ergonomics*, *58*(7), 1220–1231. https://doi.org/10.1080/00140139.2015.1005165

22. Zuska, A., Szumska, E., & Frej, D. (2021). Laboratory tests of the control of the child seats using method for the vibration comfort of children transported in them. *Communications – Scientific Letters of the University of Zilina*, *23*(3), B187–B199. https://doi.org/10.26552/com.C.2021.3.B187-B199

*Manuscript received April 1, 2026; accepted for publication July 4, 2026; published online September 1, 2026.*